Maps of Global Mean Surface Temperature (GMST) during the Phanerozoic: Combining Global Climate Modeling Results with Geological-Geochemical Estimates of Paleotemperature

Christopher R. Scotese

Department of Earth & Planetary Sciences

Northwestern University

cscotese@gmail.com

January 21, 2022

Abstract

This set of Global Mean Surface Temperature (GMST) arrays for 100 Phanerozoic time intervals (stage level) are based on HadleyCM3L simulations (Valdes et al, 2021) that have been modified to better agree with geochemical proxy data (∂18O) and more equable pole-to-equator temperature gradients deduced from lithological indicators of climate (evaporites, calcrete, coals, bauxites, and tillites, etc.) (Scotese et al., 2021). The resolution is 1x1 degrees (latitude/longitude) in three formats: grid-reference, coordinate-list, and netcdf. Version: scotese02a_v21321

Introduction

Several recent studies have published estimates describing how global temperature has changed during the last 540 million years (Figure 1; Scotese et al., 2021). These temperature curves identify times when the Earth's global average temperature was much warmer than the present-day (hothouse intervals) and time intervals when, like the present-day, the Earth has been locked in a frigid "icehouse" world. Figure 2 is a "heat map" which highlights these hothouse and icehouse intervals (Scotese et al., 2021).

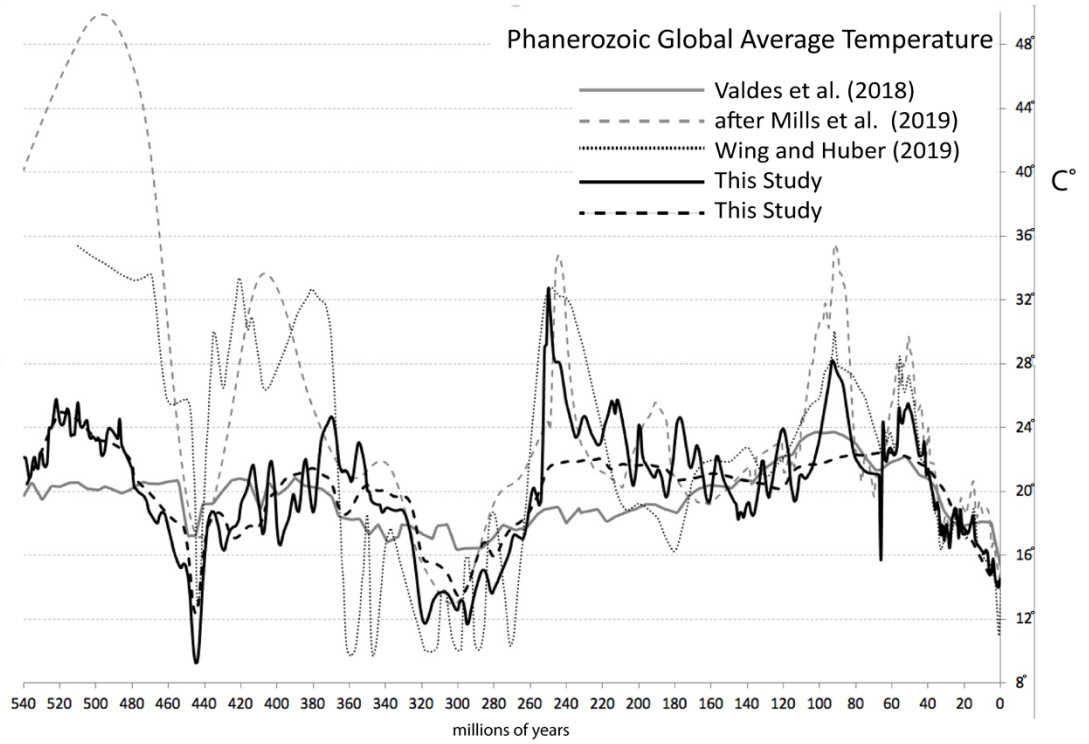

Figure 1. Estimates of Global Average Temperature during the Phanerozoic

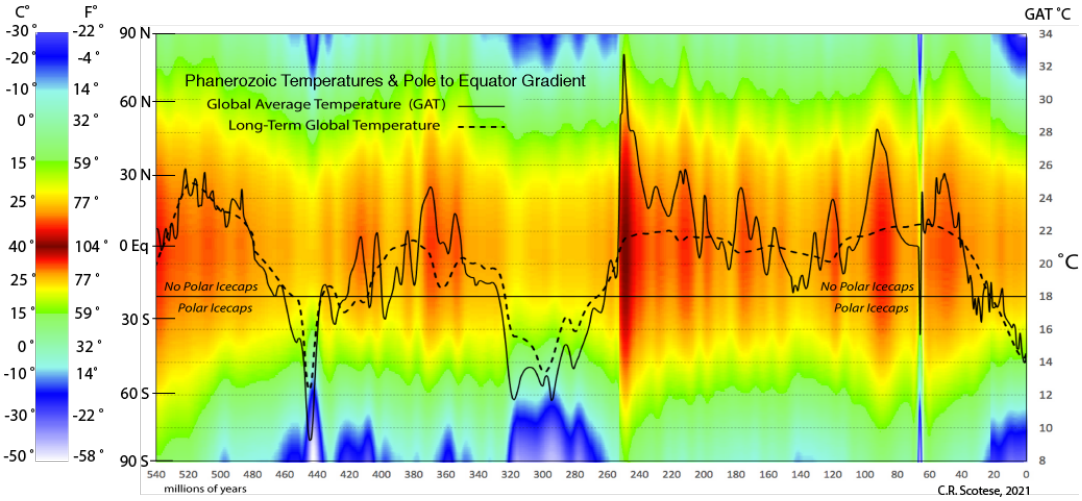

Figure 2. A geological “heat map” illustrating the changing pole-to-equator temperature

Icehouse worlds, like the present-day, are times when permanent icecaps cover the north or south poles (or both). During icehouse intervals the average global temperature is less than 18˚ C (64˚ F) and temperatures in the polar regions are frigid (-17˚ C; 0˚ F). During icehouse intervals the average temperature in the tropics rarely exceeds 26˚C (79˚ F). During the last 540 million years the Earth has been characterized by icehouse conditions approximately 25% of the time. The most intense icehouse worlds occurred during the Late Ordovician (450 Ma – 440 Ma), the Permo-Carboniferous (355 Ma – 270 Ma), and the late Cenozoic (35Ma – 0 Ma). We are currently living in an extreme icehouse world (Figure 3).

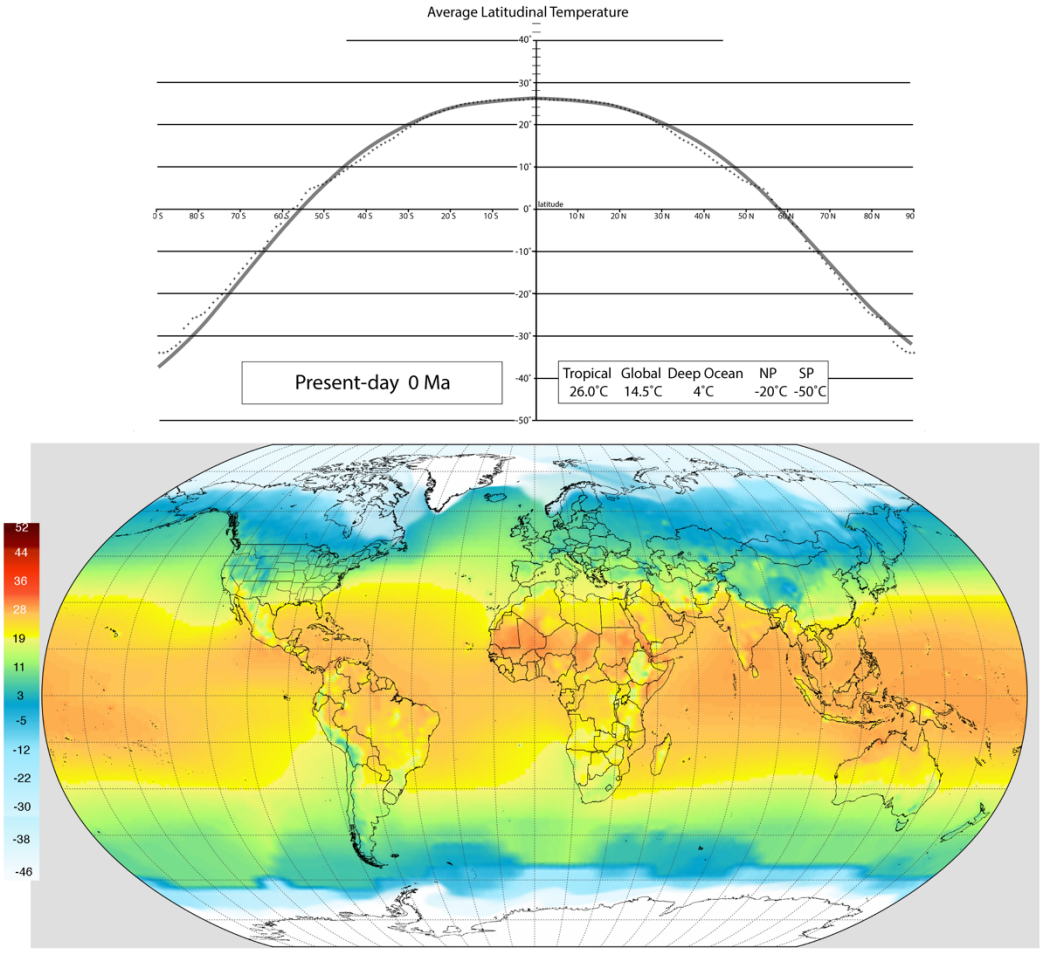

Figure 3. Present-day latitudinal temperature gradient (top), and global surface temperature map (bottom) (Legates & Wilmott, 1990).

During hothouse times the average global temperature is about 10˚ C (18˚ F) warmer than today's world and temperatures above the polar circle are relatively warm (8˚ C; 47˚F). No polar icecaps are present during hothouse intervals and warm tropical, fauna and flora inhabit the polar regions (Huber, 1998; Huber et al. 2000). During hothouse intervals, the average annual temperature in the tropics (20˚ N – 20˚S) often exceeds 30˚C (86˚F). During the last 540 million years hothouse intervals occur about 60% of the time. The most robust hothouse periods were the Early Paleozoic (540 Ma – 460 Ma), the Devonian (415 Ma – 360 Ma), the Triassic-Jurassic (250 Ma – 160 Ma), the mid Cretaceous (110 Ma – 70 Ma), and the Paleocene-Eocene (65Ma – 40 Ma). The most recent hothouse world was the late Eocene, 40 million years ago.

About 15% of the time the Earth's has been in transition between a hothouse and icehouse world. During these time intervals, positive feedback mechanisms such as changes in the reflectivity of the Earth's surface due to the waxing and waning of polar ice caps (10,000 – 100,000 years), can rapidly change the Earth's average temperature. The Earth is currently experiencing a rapid, man-made transition from an icehouse to a hothouse world. It is very likely that during the next ~150 years the Earth's temperature will rise by ~4.5˚C (8˚F) (Figure 4; Scotese, 2020; Scotese et al., 2021). A new equilibrium temperature of 19˚C (67˚F) will be will be attained in the next 5,000 - 10,000 thousand years (Archer 2009, Archer et al., 2009). After global warming, the North Polar and Greenland ice caps will have melted and the Antarctic ice cap will be much reduced. Sea level will have risen, ~100 meters flooding 10% of the low-lying regions of the continents (Figure 5).

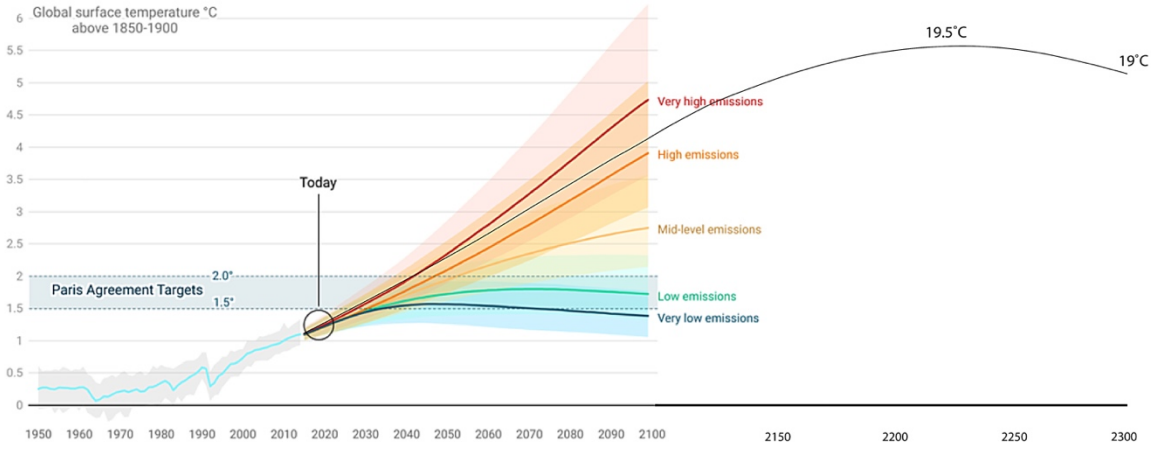

Figure 4. Projection of future global warming (2020 – 2100, IPCC (2021); 2100-2300, Scotese (2020), Scotese et al. (2021)). Global warming levels off at 19.5˚C during the early 2200's due to the depletion of fossil fuels BP(2019), Shell (2018).

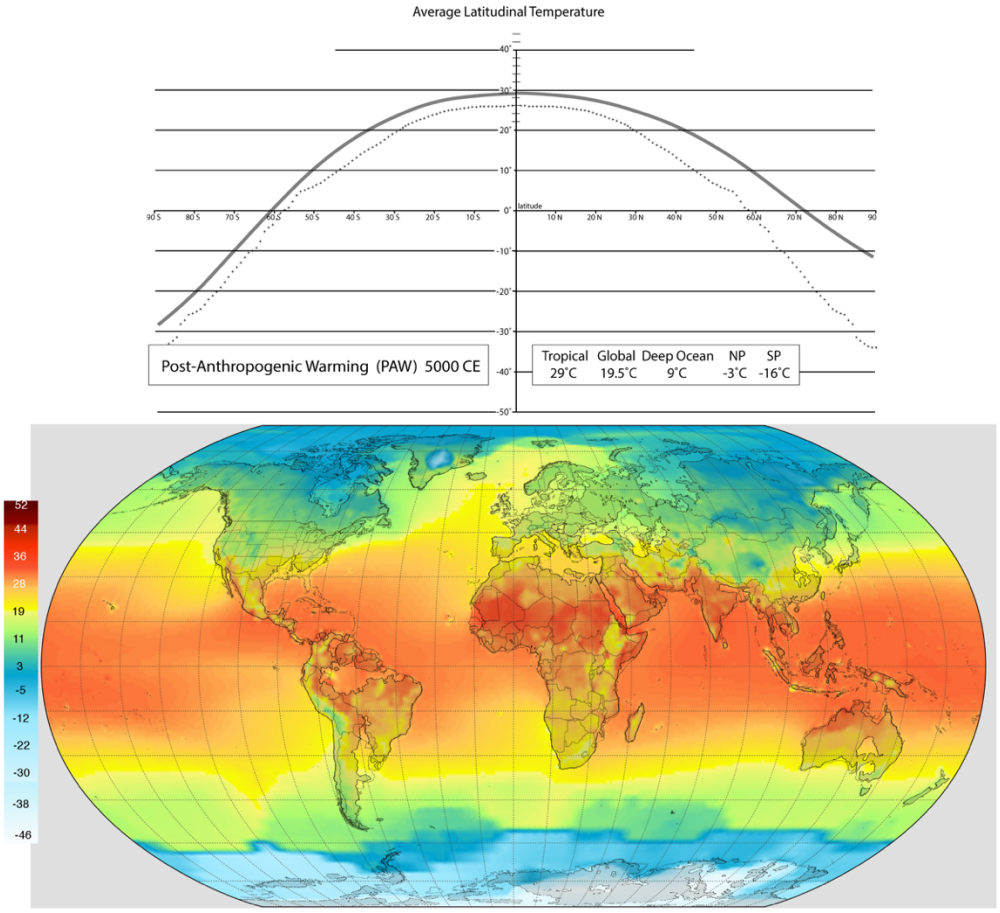

Figure 5. Post-Anthropogenic Global Warming (~5000 CE), latitudinal temperature gradient (top), and global temperature map (bottom). Global Temperatures stabilize at 19˚C (Scotese, 2019; Scotese et al., 2021). The dotted line is the present-day temperature gradient. The black line landward of the modern coastlines indicates areas of the continents will flooded by the ocean.

Compare Figure 5 to Figure 3. Note that equatorial temperatures will have risen ~3˚ C (8˚F). Future temperatures will increase even more dramatically in the polar regions. The temperature at 60˚N will be 10˚C (18˚F) warmer than present-day. The last time the world was this warm was during the late Eocene, 40-35 million years ago, when the glaciers flowing from the expanding Antarctic ice cap had just begun to reach the sea (Koeberl & Montanari, 2009; Ruddiman, 2001; p. 148).

Constructing Paleotemperature Maps for Deep Time

GCM's rely on estimates of the concentration of atmospheric CO_2 to model paleotemperature

In order to create a global paleotemperature map it is necessary to model how atmospheric circulation, ocean circulation, and mountains effect regional temperature. Decades of modeling experience has produced Global Climate Models (GCMs) that very accurately simulate the motions of atmosphere and oceans. However, the day-to-day motion of the atmosphere and ocean tells us very little about the changes in global temperature that occur over hundreds of thousands or millions of years.

It is a well-known fact that CO_2 is a greenhouse gas and has played an important, if not the predominant role, in regulating the Earth's temperature through time. To modulate global temperature, GCMs rely on estimates of the ancient level of atmospheric CO_2. Very simply stated: higher concentrations of CO_2 lead to higher global temperatures; lower concentrations of

CO_2 lead to cooler global temperatures. An accurate estimate of the ancient concentration of atmospheric CO_2 is essential if we are to successfully model past climates.

There have been only a few studies that have attempted to describe the variation in atmospheric CO_2 during the past 540 million years. One of the more recent efforts by Foster et al. (2017) uses CO_2 proxy data compiled by Dana Royer (Wesleyan University) to produce a curve that illustrates how the atmospheric concentration of CO_2 has fluctuated during the past 420 million years (red line – Figure 6). The Foster curve, however, suffers from gaps in the CO_2 record and time intervals when the CO_2 estimates vary widely.

These data gaps are especially large in the early and middle Paleozoic (460 Ma – 320 Ma), the late Permian and early Triassic (270 Ma – 230 Ma), and the mid-Jurassic (180ma – 150 Ma). There is no reliable data for the Cambrian and early Ordovician (540Ma – 460 Ma). The proxy values for CO_2 are quite variable during the early Permian (360 ppm – 1440 ppm), the Triassic (400 ppm – 3240 ppm), and the Paleocene (360 ppm – 1200 ppm).

In order to improve the estimates of CO_2, we have used our growing understanding of the temperature history of the Phanerozoic (Scotese et al., 2021) to refine and update the Foster CO_2 curve. The sequence of black and white intervals along the time axes refer to times of global warming (black) and global cooling (white). Most of the CO_2 peaks in the Foster curve correspond with warm intervals, but not all of them. Assuming CO_2 is the predominant cause of global warming, it is reasonable to redraw the CO_2 curve so that peaks in the CO_2 curve correspond with warm intervals.

By considering an independent estimate of temperature, we can now "fill in the gaps" and reject contradictory CO_2 data. For example, during the Triassic and the late Cretaceous, CO_2 estimates less than ~1080 ppm were rejected (open circles).

At first this may seem like circular reasoning. However, no CO_2 proxy data was used to determine the cool and warm intervals (Scotese et al., 2021). We are simply redrawing the CO_2 curve so that it conforms with what we independently know about global temperature change. As can be seen by visual inspection of Figure 6, the goodness of fit between the revised CO_2 curve and the CO_2 proxy data improves significantly as a result of the rejection of questionable CO_2 values.

However, this is not a final answer. There are still large gaps in the CO_2 proxy record. The estimation of some of the CO_2 peaks where there are few data points (i.e., Cambrian, early Triassic, Cenomanian-Turonian), is speculative. . This curve, however, represents a testable hypothesis that awaits conformation or rejection with additional data.

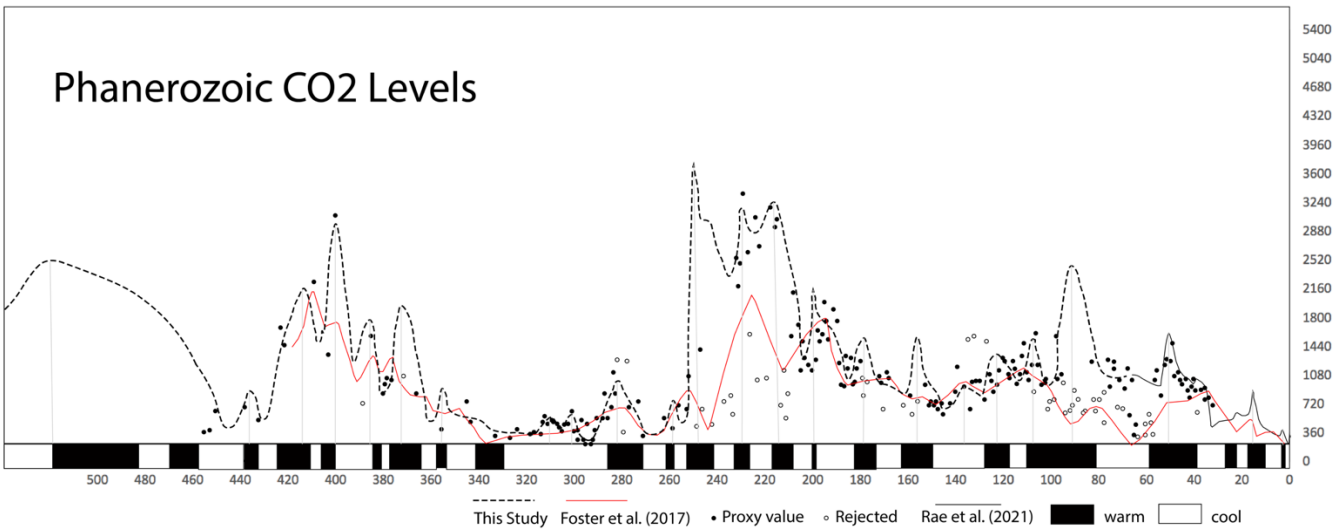

Figure 6. Phanerozoic CO_2 Levels. Black dots – Average CO_2 measurements binned by 1 million-year intervals. Open circles – rejected CO_2 measurements. The red line is the CO_2 estimates of Foster et al. (2017). The gray line is the Cenozoic CO_2 estimates of Rae et al. (2021). The black and white rectangles indicate "warm" (black) and "cool" (white) time intervals (Scotese et al., 2021). A vertical gray line connects warm intervals with the proposed peaks in the CO_2 curve.

Now that we have described how the amount of CO_2 in the atmosphere has changed through time, we can use these estimates to run GCM simulations of past climate. These GCM-derived estimates of paleotemperature can then be compared with other paleotemperature estimates obtained from the geological and fossil record (Parrish, 1998; Boucot et al., 2013) as well as direct geochemical measurements of paleotemperature (Veizer and Prokoph, 2015; Mills et al., 2019; Song et al., 2019; Grossman and Joachimski, 2020; Scotese et al., 2021) .

Comparing Estimates of Paleotemperatures from GCMs with Paleotemperatures from Geological and Geochemical Models

In recent years, two independent estimates of Phanerozoic paleotemperatures have been made: 1) Global Climate Simulations (Valdes et al., 2021) and 2) based on the geological record combined with geochemical estimates of paleotemperature using oxygen isotopes (Scotese et al., 2021). These two methodologies are completely independent and though the resulting temperature curves are similar, there are important differences that are worth discussing.

As the name implies, Global (or General) Circulation Models are sophisticated mathematical models run on supercomputers that use basic physics to simulate the motion of the atmosphere and oceans (Valdes et al., 2021). As discussed in the previous section, an estimate of CO_2 levels is used by these computer simulations to modulate paleotemperature. In contrast, the geological-geochemical model of paleotemperature is entirely data driven. The paleogeographic distribution of lithologic indicators of climate, such as coals, bauxites, evaporites, and tillites (Boucot et al., 2013), combined with geochemical measurements of paleotemperature, primarily oxygen isotopes (Song et al., 2019; Grossman & Joachimski, 2020) are used to estimate the temperature of the tropics and the latitudinal variation of temperature from the pole to the equator. Figure 7 illustrates a typical geological-geochemical paleotemperature diagram, in this case for the Maastrichtian, 70 million years ago. The small circles and plus signs plotted along the curve are

the estimates of paleotemperature derived from oxygen isotopic measurements (Song et al., 2019).

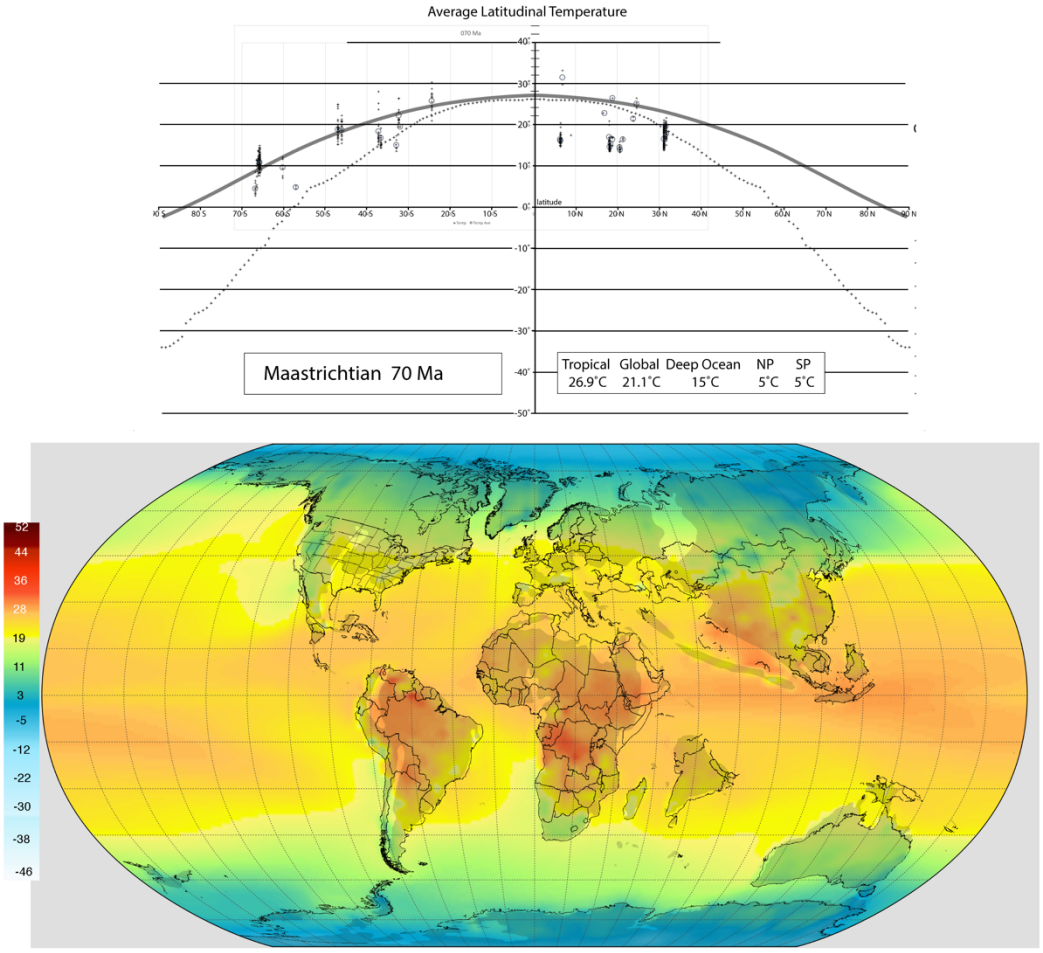

Figure 7. Late Cretaceous (Maastrichtian, 70 Ma) latitudinal temperature gradient (top), and temperature map (bottom). Global Average Temperature is 21.1˚ C (Scotese et al., 2021). The dotted line is the present-day temperature gradient. The small circles and plus signs are measurements of paleotemperature derived from oxygen isotopic measurements (Song et al., 2019).

The results of these two independent estimates of global paleotemperature can be compared in Figure 8. Figure 8A is the geological-geochemical estimate of Phanerozoic paleotemperature (see also Figure 2). Figure 8B is a comparable "heat map" based on the HadleyCM3 computer simulation of paleoclimate (Valdes et al., 2021). This climatic simulation uses the CO_2 curve of Foster et al. (2017) to modulate global temperature. The broad features of the two curves are

similar. Both show the classic "double-humped" temperature pattern (Fischer, 1984; Summerhayes, 2015). An early-mid Paleozoic hothouse interval (540 Ma – 340 Ma) is separated from a Mesozoic hothouse interval (250 Ma – 40 Ma) by a Permo-Carboniferous icehouse (340 Ma – 250 Ma). Both curves indicate a brief ice age during the latest Ordovician (Hirnantian Ice Age) and both curves end with rapid cooling during the Late Cenozoic Ice Age (40 Ma – 0 Ma; Zachos et al., 2008).

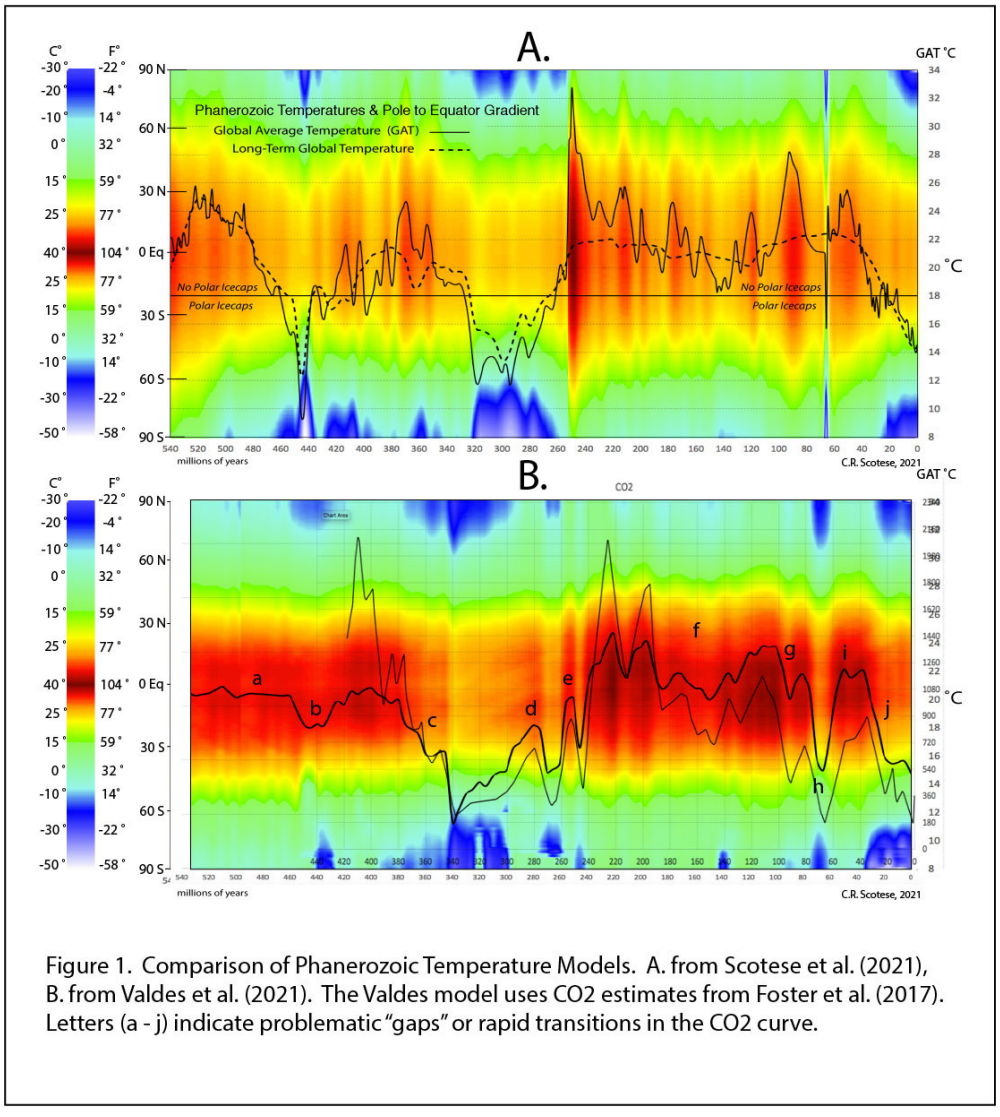

Figure 1. Comparison of Phanerozoic Temperature Models. A. from Scotese et al. (2021), B. from Valdes et al. (2021). The Valdes model uses CO2 estimates from Foster et al. (2017). Letters (a - j) indicate problematic "gaps" or rapid transitions in the CO2 curve.

Figure 8. A comparison of the "geological-geochemical" heat map (A, Scotese et al., 2021), with the "heat map" derived from computer simulations (B, HadleyCM3; Valdes et al., 2021). Note how the temperature curve tracks the CO levels in B (thin black line). a- no reliable CO_2 data prior to 460 Ma, b- The Hirnantian Ice Age is muted, c- Famennian temperature drop is too early, d- anomalous temperature high during the Permo-Carboniferous glacial

maximum, e- earliest Triassic thermal maximum is missing, f- few CO_2 proxy data available for this interval , g- Cenomanian-Turonian thermal maximum is much too low, h- latest Cretaceous cool period too long and too cool, i- wide range of conflicting CO_2 values, j- Cenozoic Ice Age fall is delayed ~15 my .

Most of the differences in the shapes of the two curves can be attributed to the problems with previous estimates of CO_2 alluded to in the previous section. These problematic time intervals are labeled "a" through "j" are described in the caption to Figure 8.

In addition to differences in the shapes of the paleotemperature curves (black lines), the two "heat maps" are substantially different. The Valdes heat map has brighter and darker reds indicating warmer temperatures in the tropics and has cooler greens and blues at mid to high latitudes. In the Scotese heat map, there is distinct alternation between warmer and cooler periods, and there is a higher frequency and amplitude of temperature change.

It is worthwhile exploring the differences between the two climate models in more detail. If we take a deeper dive into one "time-slice", we can see that the predicted range of latitudinal temperatures is quite different. Figure 9 compares the pole-to-equator latitudinal gradient in temperature produced by geological-geochemical (9A) and the HadleyCm3 GCM (9B.

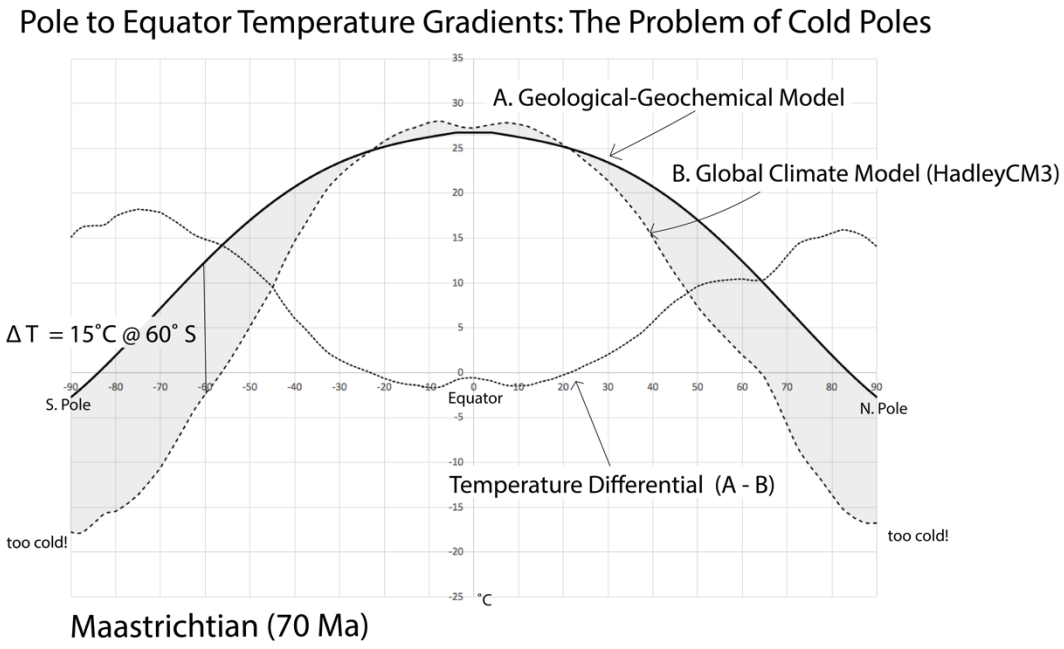

Figure 9. Comparison of pole-to-equator temperature gradients produced by the (A) Geological-Geochemical Model (Scotese et al., 2021), and the Global Climate Model (HadleyCM3), Valdes et al., 2021). The broad u-shaped dotted line is the temperature differential between the two curves.

The area of gray shading between the two curves is the difference in temperatures predicted by the two models. This difference is especially notable at mid to high latitudes. It has been long recognized polar temperatures predicted by the computer simulations tend to be colder than expected (Upchurch et al., 2015). This is sometimes referred to as the "Cold Poles Problem".

As noted in Figure 8, the GCM results are "hotter" in the tropics (deep reds) and cooler at higher latitudes (more light blues). Another way to state the "Cold Poles Problem" is that the GCMs do not have an easy time modeling "equability" (Huber et al., 2011; McInerny & Wing, 2011). Equability is short-hand for a reduced pole-to-equator temperature gradient. The modern pole-to-equator temperature gradient is ~.8˚ C per one degree of latitude. For example, if the temperature at 30˚ latitude is 20˚C, then the predicted temperature at 70˚ would be -12˚C, which is old enough

to form permanent ice caps. A temperature gradient of .8˚C per 1˚ latitude is typical of icehouse worlds.

A hothouse world is more “equable” meaning the pole-to-equator temperature gradient is more reduced, typically ~.4˚C per 1˚ latitude. For example, if the temperature at 30˚ latitude is 24˚C, then the predicted temperature at 70˚ latitude would be 8˚C, which is well above freezing. A temperature gradient of .4˚C per 1˚ latitude is typical of hothouse worlds.

As illustrated in Figure 9, a typical icehouse pole-to-equator gradient is “steep” (dashed line), whereas a hothouse pole-to-equator gradient is “flat” (solid line). As noted earlier, the inability of GCMs to model flat, more equable pole-to-equator gradients results in both somewhat higher equatorial temperatures and cooler temperatures at higher latitudes. This problem had been noted by climate modelers and modifications to the simulation are being made that result in warmer temperatures at mid to high latitudes (P. Valdes personal communication).

However, there is a solution to this dilemma. We can combine our estimate of the pole-to-equator temperature gradient determined from geological and geochemical record (Figure 9A) with the relative changes in temperature across the globe provided by climate simulations.

This is a two-step process. In the first step, the temperature differential is calculated at each latitude. For example, in Figure 9, the temperature at 60˚S is 12˚C on the geological-geochemical curve and is -3˚C on the GCM curve. This gives a temperature differential of 15˚C . This temperature differential can be used to “correct” or “adjust” the GCM results. It should be noted that the magnitude of the temperature adjustment is not constant and changes as a function of latitude. In general, negative corrections will be applied GCM temperature estimates in tropical latitudes, making the GCM temperature estimates a little “cooler”, and positive corrections will be applied GCM estimates of temperature in mid to high latitudes making the GCM temperature estimates “warmer”.

In the second and final step, the latitudinal temperature differential is added to each temperature grid cell in the temperature map produced by the GCM simulation. This adjustment will not affect the relative changes in temperature along each line of latitude, but will systematically adjust the pole-to-equator temperature gradient over the entire map. Figure 10 illustrates the global temperatures "before" and "after" the application of this differential temperature adjustment. Tropical temperatures are very similar but the mid to high latitude areas are 5˚ - 10˚ C warmer after the correction has been made. The complete Maastrichtian (70Ma) global temperature map "after adjustment" is shown in Figure 7. In the Supplemental Materials, we provide an additional 100 paleotemperature maps for every stage during the Phanerozoic that were produced using this methodology. These data files and maps can be downloaded at "XXX insert link hereXXX".

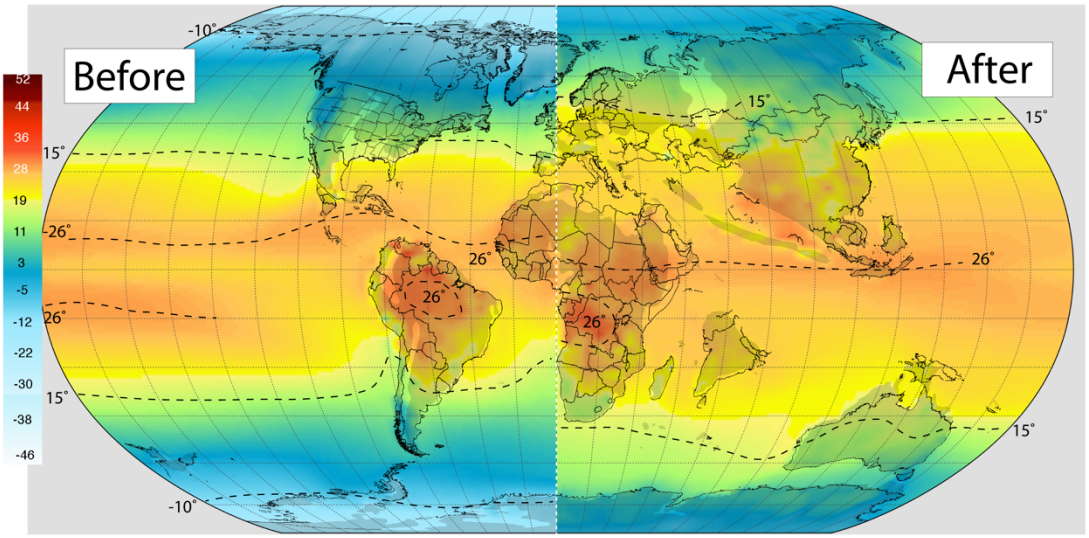

Figure 10. Comparison of global temperatures "before" and "after' the application of the latitudinal temperature adjustment. For the complete "after adjustment" map see Figure 7 (Late Cretaceous, Maastrichtian, 70 Ma).

References Cited

Archer, D., 2009. The Long Thaw, How Humans Are Changing the Next 100,000 years of Earth's Climate, Princeton University Press, Princeton, 180 pp.

Archer, D., Eby, M., Brovkin, V., Ridgwell, A., Cao, I., Mikolajewicz, U., Caldiera, K., Matsumoto, K., Munhoven, G., Montenegro, A., and Tokos, K., 2009. Atmospheric lifetime of fossil fuel carbon dioxide, Annual Review of Earth and Planetary Sciences, v. 37, pp. 117-134.

Boucot, A.J., Chen Xu, and Scotese, C.R, 2013. Phanerozoic Paleoclimate: An Atlas of Lithologic Indicators of Climate, SEPM Concepts in Sedimentology and Paleontology, (Print-on-Demand Version), No. 11, 478 pp., ISBN 978-1-56576-289-3, October 2013, Society for Sedimentary Geology, Tulsa, OK.

British Petroelum (BP), 2019, "BP Energy Outlook, 2019". https://www.bp.com/content/dam/bp/business-sites/en/global/corporate/pdfs/energy-economics/energy-outlook/bp-energy-outlook-2019.pdf

Fischer, A. G., 1984. The Two Phanerozoic Supercycles, in Catastrophes and Earth History: The New Uniformitarianism, W.A. Berggren and J.A. Van Couvering, (editors), Chapter 7, Princeton University Press, Princeton, N.J., pp. 129 – 150.

Foster, G.L., Royer, D.L., and Lunt, D.J., 2017. Future Climate Forcing Potentially without precedent in the last 420 million years, Nature Communications, v. 8, 14845, doi:10.1038/ncomms14845.

Grossman, E.L., and Joachimski, M.M., 2020. Oxygen Isotope Stratigraphy, Chapter 10, in The Geologic Time Scale 2020, F. M. Gradstein, J.G. Ogg, M.D. Schmitz, and G.M. Ogg (editors), Elsevier, Amsterdam, volume 1, (in press).

Huber, B.T., 1998. Tropical paradise at the Cretaceous poles?, Science, v. 282, p. 2199-2200.

Huber, B.T., MacLeod, K.G., and Wing, S.L., 2000. Warm Climates in Earth History, Cambridge University Press, 462 pp.

Huber, M., and Caballero, R., 2011. The early Eocene equable climate problem revisited: Climate of the Past Discussions, v.7., p. 241-304, doi: 10.5194/cpd-7-241-2011.

IPCC, 2021. Summary for Policymakers. In: *Climate Change 2021: The Physical Science Basis. Contribution of Working Group I to the Sixth Assessment Report of the Intergovernmental Panel on Climate Change* [Masson-Delmotte, V., P. Zhai, A. Pirani, S. L. Connors, C. Péan, S. Berger, N. Caud, Y. Chen, L. Goldfarb, M. I. Gomis, M. Huang, K. Leitzell, E. Lonnoy, J.B.R. Matthews, T. K. Maycock, T. Waterfield, O. Yelekçi, R. Yu and B. Zhou (eds.)]. Cambridge University Press.

Koeberl, C., and Montanari, A., 2009. The Late Eocene Earth: Hot House, Ice House, and Impacts, Geol. Soc. America, Special Paper 452, Boulder, Colorado, 322 pp.

Lécuyer, C., Amiot, R., Touzeau, A., 2013. Calibration of the phosphate $\delta^{18}O$ thermometer with carbinate-water oxygen isotope fractionation equations, Chemical Geology, v. 347, pp. 217-226, doi:10.13039/501100004794.

Legates, D.R., and Wilmott, C.J., 1990. Mean seasonal and spatial variability in global surface air temperature, Theoretical and Applied Climatology, v. 41, pp. 11-21.

McInerney, F.A., Wing, S.L., 2011. The Paleocene-Eocene Thermal Maximum: a perturbation of carbon cycle, climate, and biosphere with implications for the future. Annual Review of Earth Planetary Sciences,v. 39, p. 489–516.

Mills, B.J.W., Krause, A.J., Scotese, C.R., Hill, D.J., Shields, G.A., and Lenton, T.M., 2019. Modelling the long-term carbon cycle, atmospheric CO_2, and Earth surface temperature from late Neoproterozoic to present-day, Gondwana Research, v. 67, p. 172-186, doi: 10.1016/j.gr.2018.12.001 1342-937.

Parrish, J.T., 1998. Interpreting Pre-Quaternary Climate from the Geologic Record, Columbia University Press, New York, 338 pp.

Rae, J.W.B., Zhang, Y.G., Liu, X., Foster, G.L., Stoll, H.M., and Whiteford, 2021. Atmospheric CO2 over the Past 66 Million Years from Marine Archives, Annual Review of Earth and Planetary Sciences, 49: 609-41.

Ruddiman, W.F., 2001. Earth's Climate: Past and Future, W.H. Freeman and Company, New York, NY, 465 pp.

Scotese, C.R., 2016. A New Global Temperature Curve for the Phanerozoic, (abstract), Geological Society of America Annual Meeting, Sunday, September 25, 2016, Session no. 74, #287, Recent Advances in Paleoclimatology and Paleoceanography (Posters). Exhibit Hall E/F (Colorado Convention Center), Geological Society of America Annual Meeting, Denver, CO.

Scotese, C.R., 2020. Global Warming during the next 300 years, A Global Warming Calculator (student exercise with Excel spreadsheet), PALEOMAP Project, Evanston, IL. 49 pp.

Scotese, C.R., Song, H., Mills, B.J.W., and van der Meer, D., 2021. Phanerozoic Paleotemperatures: The Earth's Changing Climate during the last 540 million years, Earth-Science Reviews, https:/doi.org/10.1016/j.earscirev.2021.103503.

Shell (2018), Shell Scenarios: SKY, Meeting the Goals of the Paris Agreement, https://www.shell.com/promos/business-customers-promos/download-latest-scenario-sky/_jcr_content.stream/1530643931055/eca19f7fc0d20adbe830d3b0b27bcc9ef72198f5/shell-scenario-sky.pd

Song, H., Wignall, P.B., Song, H., Dai, X., and Chu, D., 2019. Seawater temperature and dissolved oxygen over the past 500 million years, Journal of Earth Sciences, v.30, no. 2, p. 236-243, doi:10.1007/s12583-028-1002-2.

Summerhayes, C.P.,2015. Earth's Climate Evolution, Wiley-Blackwell, Chichester, UK, 394 pp.

Upchurch, G.R., Kiehl, J., Shields, C., Scherer, J., and Scotese, C.R., 2015. Latitudinal temperature gradients and high latitude temperatures during the latest Cretaceous: Congruence of geologic data and climate models, Geology, v. 43, no. 9, p. 683-686.

Valdes, P.J., Scotese, C.R., and Lunt, D.J., 2021. Deep Ocean Temperatures Through Time, Climate of the Past, v. 17, p. 1483-1506, https://doi.org/10.5194/cp-17-1483-2021

Veizer. J.T., and Prokoph. A., 2015. Temperatures and Oxygen isotopic composition of Phanerozoic oceans, Earth-Science Reviews, v. 146: p. 92-104, doi: 10.1016/j.earscirev.2015.03.008.

Wing, S., and huber, B., 2019. Earth's Temperature History Workshop, Smithsonian Institution, National Museum of Natural History, March 30-31, 2018, Washington, D.C.

Zachos, J.C., Dickens, G.R., and Zeebe, R.E., 2008. An early Cenozoic perspective on greenhouse warming and carbon-cycle dynamics, Nature, v. 45117, p. 279-283.